



HAL
open science

Physical mechanisms controlling the initiation of convective self-aggregation in a General Circulation Model

David Coppin, Sandrine Bony

► **To cite this version:**

David Coppin, Sandrine Bony. Physical mechanisms controlling the initiation of convective self-aggregation in a General Circulation Model. *Journal of Advances in Modeling Earth Systems*, 2015, 7 (4), pp.2060-2078. 10.1002/2015MS000571 . hal-01276368

HAL Id: hal-01276368

<https://hal.sorbonne-universite.fr/hal-01276368>

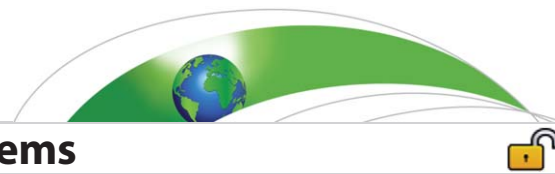
Submitted on 19 Feb 2016

HAL is a multi-disciplinary open access archive for the deposit and dissemination of scientific research documents, whether they are published or not. The documents may come from teaching and research institutions in France or abroad, or from public or private research centers.

L'archive ouverte pluridisciplinaire **HAL**, est destinée au dépôt et à la diffusion de documents scientifiques de niveau recherche, publiés ou non, émanant des établissements d'enseignement et de recherche français ou étrangers, des laboratoires publics ou privés.



Distributed under a Creative Commons Attribution - NonCommercial - NoDerivatives 4.0 International License



RESEARCH ARTICLE

10.1002/2015MS000571

Physical mechanisms controlling the initiation of convective self-aggregation in a General Circulation Model

David Coppin¹ and Sandrine Bony¹

¹Sorbonne Universités, UPMC Univ Paris 06, CNRS, LMD/IPSL, Paris, France

Key Points:

- Temperature dependence of convective self-aggregation in a GCM
- The physical mechanisms that initiate aggregation depend on temperature
- Low-cloud sensitivity to SST contributes to a large extent to the SST dependence of aggregation

Correspondence to:

D. Coppin,
david.coppin@lmd.jussieu.fr

Citation:

Coppin, D., and S. Bony (2015), Physical mechanisms controlling the initiation of convective self-aggregation in a General Circulation Model, *J. Adv. Model. Earth Syst.*, 7, 2060–2078, doi:10.1002/2015MS000571.

Received 23 OCT 2015

Accepted 4 DEC 2015

Accepted article online 13 DEC 2015

Published online 30 DEC 2015

Abstract Cloud-resolving models have shown that under certain conditions, the Radiative-Convective Equilibrium (RCE) could become unstable and lead to the spontaneous organization of the atmosphere into dry and wet areas, and the aggregation of convection. In this study, we show that this “self-aggregation” behavior also occurs in nonrotating RCE simulations performed with the IPSL-CM5A-LR General Circulation Model (GCM), and that it exhibits a strong dependence on sea surface temperature (SST). We investigate the physical mechanisms that control the initiation of self-aggregation in this model, and their dependence on temperature. At low SSTs, the onset of self-aggregation is primarily controlled by the coupling between low-cloud radiative effects and shallow circulations and the formation of “radiatively driven cold pools” in areas devoid of deep convection, while at high SSTs it is primarily controlled by the coupling between surface fluxes and circulation within convective areas. At intermediate temperatures, the occurrence of self-aggregation is less spontaneous and depends on initial conditions, but it can arise through a combination of both mechanisms. Through their coupling to circulation and surface fluxes, the radiative effects of low-level clouds play a critical role in both initiation mechanisms, and the sensitivity of boundary layer clouds to surface temperature explains to a large extent the temperature dependence of convective self-aggregation. At any SST, the presence of cloud-radiative effects in the free troposphere is necessary to the initiation, growth, and maintenance of convective aggregation.

1. Introduction

Observations show that tropical convection can exhibit a large diversity of organizations, ranging from random distribution of convective clouds to mesoscale convective systems [Houze, 2004], squall lines, and hurricanes to planetary-scale organization such as large superclusters [Nakazawa, 1988; Mapes and Houze, 1993] or the Madden-Julian Oscillation (MJO) [Madden and Julian, 1994]. The mechanisms leading to such organizations have long been studied using a hierarchy of numerical models. In a pioneer study using a two-dimensional Cloud-Resolving Model (CRM), Held *et al.* [1993] showed that under certain conditions, the atmosphere could spontaneously develop narrow and stationary deep convective regions surrounded by dry subsiding areas. This was the very first example of what is now called convective self-aggregation. In a later study, Tompkins and Craig [1998] ran a 3-D CRM on a small (100 km × 100 km) domain and found that convection organized itself into a band structure. Since then, many studies using CRMs over increasingly large domains have analyzed the self-aggregation phenomenon and sparked interest in the community by suggesting that this phenomenon might help us understand or revisit our interpretation of different aspects of tropical meteorology and climate [e.g., Bretherton *et al.*, 2005; Nolan *et al.*, 2007; Khairoutdinov and Emanuel, 2010; Muller and Held, 2012; Jeevanjee and Romps, 2013; Wing and Emanuel, 2014; Muller and Bony, 2015; Wing and Cronin, 2015].

Through sensitivity studies, a range of analysis methods and mechanism-denial experiments, these studies have pointed out the role of a few physical mechanisms in the initiation of convective self-aggregation. These mechanisms include couplings between surface turbulent fluxes and surface wind anomalies associated with convection (a mechanism often referred to as WISHE for Wind-Induced Surface Heat Exchange), between radiation (from clear sky and/or cloudy sky) and circulation, and between convection and humidity [e.g., Tompkins and Craig, 1998; Tompkins, 2001; Bretherton *et al.*, 2005; Nolan *et al.*, 2007; Muller and Held, 2012; Wing and Emanuel, 2014; Emanuel *et al.*, 2014; Muller and Bony, 2015; Wing and Cronin, 2015]. However, the relative role of the different mechanisms appears to be model dependent.

© 2015. The Authors.

This is an open access article under the terms of the Creative Commons Attribution-NonCommercial-NoDerivs License, which permits use and distribution in any medium, provided the original work is properly cited, the use is non-commercial and no modifications or adaptations are made.

Several CRM studies have also highlighted a dependence of convective organization on SST. For example, *Held et al.* [1993] found that convection organizes more slowly at low SSTs and *Nolan and Rappin* [2008] noticed a faster spontaneous cyclogenesis at high SST. An SST dependence of self-aggregation was also observed in *Khairoutdinov and Emanuel* [2010] and *Wing and Emanuel* [2012], with self-aggregation occurring only above 300 K but not at 310 K or above [Wing and Emanuel, 2012]. This dependence was interpreted by *Emanuel et al.* [2014] as an instability of the ordinary RCE state above a critical SST, leading either to a dry state with large-scale descent, or to a moist state with mean ascent. They also showed that the system exhibited a strong hysteresis: once convection is aggregated, it can remain in this state even if conditions become less favorable (e.g., below the critical SST) [Khairoutdinov and Emanuel, 2010; Muller and Held, 2012]. In simulations performed in a long channel geometry, *Wing and Cronin* [2015] showed evidence for a strong dependence of self-aggregation on surface temperature and pointed out the role of cloud-radiative feedbacks in this dependence.

Beyond the question of what explains the self-aggregation phenomenon, the question arises as to whether or not convective aggregation has an impact on climate [Bony et al., 2015]. *Held et al.* [1993] and *Bretherton et al.* [2005] showed that the degree of aggregation of convection had a significant impact on the large-scale state of the atmosphere, a more aggregated convection being associated with a warmer and drier troposphere. This result is consistent with observations [Tobin et al., 2012, 2013], showing that for similar surface and large-scale dynamical forcings, situations where convection is more aggregated are associated with a lower free-tropospheric humidity, less upper-tropospheric clouds, more outgoing longwave (LW) radiation, and a lower planetary albedo or reflected shortwave (SW) radiation at the top of the atmosphere.

This raises questions about the potential impact of changes in convective aggregation on climate sensitivity [Khairoutdinov and Emanuel, 2010; Mauritsen and Stevens, 2015]. Furthermore, it has been suggested that modes of variability of the tropical atmosphere such as the Madden-Julian Oscillation (MJO) could be a large-scale manifestation of convective aggregation [Khairoutdinov and Emanuel, 2012]. This idea is supported by observations showing that the MJO develops in an area where the organization of convection tends to promote the development of large-scale ascents [Tobin et al., 2013], and by a numerical study showing that MJO and self-aggregation exhibit similar budgets of moist static energy (MSE) and are supported by the same diabatic feedbacks [Arnold and Randall, 2015].

Finally, it has been proposed that tropical cyclones could represent a particular case of convective aggregation, as convective aggregation often gives rise to tropical cyclones in simulations performed in the presence of rotation [Nolan et al., 2007; Held and Zhao, 2008; Khairoutdinov and Emanuel, 2013; Shi and Bretherton, 2014].

Providing that GCMs exhibit some self-aggregation behavior [Held et al., 2007; Shi and Bretherton, 2014; Reed et al., 2015; Arnold and Randall, 2015], they would constitute convenient tools to investigate the role that this behavior plays in the global climate. Pioneering studies carried out by *Held et al.* [2007], *Held and Zhao* [2008], and *Popke et al.* [2013] have shown that GCMs run in an RCE configuration offered a great potential to study the fundamental processes that control large-scale circulations, and *Held et al.* [2007], *Reed et al.* [2015], *Arnold and Randall* [2015], as well as *Becker and Stevens* [2014] have shown that the GFDL, NCAR, and MPI GCMs run in this configuration exhibited some form of self-organization. In this study, we study the self-aggregation behavior using the IPSL-CM5A-LR atmospheric GCM run in RCE for a range of prescribed SSTs. Section 2 presents the model setup and describes the dependence of self-aggregation on SST and initial conditions. Section 3 introduces the analysis framework used to analyze the physical processes responsible for the initiation of self-aggregation, and discusses the dependence of these processes on SST.

Sections 4 and 5 analyze in detail the triggering mechanisms of convective aggregation at low and high SSTs, respectively, and section 6 examines the case of intermediate SSTs. Section 7 summarizes the key findings and discusses the similarities and differences between our results and those obtained with other models.

2. Model Setup and Dependence of Self-Aggregation on SST

2.1. Radiative-Convective Equilibrium Simulations

We use the LMDZ5A GCM [Hourdin et al., 2006], the atmospheric component of the IPSL-CM5A-LR coupled ocean-atmosphere model [Dufresne et al., 2013] that participated in the fifth phase of the Coupled Model

Intercomparison Project (CMIP5). This model has a horizontal resolution of $3.75^\circ \times 1.875^\circ$ in longitude-latitude and 39 levels on the vertical (15 in the stratosphere). Its physical package [Hourdin *et al.*, 2012] includes the Emanuel convection scheme [Emanuel, 1993], a statistical cloud scheme coupled to the convection scheme [Bony and Emanuel, 2001], a radiative transfer code [Morcrette, 1991], and a parameterization of the boundary layer as a diffusion with an eddy diffusivity which depends on the local Richardson number and handles dry convection in the case of unstable profiles [Deardorff, 1972]. Gravity wave drag is calculated following Lott [1999]. For a more detailed review of LMDZ5A-LR GCM, readers are referred to Hourdin *et al.* [2006] and Dufresne *et al.* [2013], and references therein.

To run RCE simulations, we use the model in an aquaplanet configuration without rotation, and employ a latitudinal discretization on a sinusoidal grid to ensure that the grid mesh area is uniform over the globe. The model is forced by a constant and uniform insolation (1066.78 W/m^2 with a zenith angle of 0° and a diurnal cycle) and a prescribed uniform SST. The ocean albedo is set to 0.07. The stratospheric ozone distribution is invariant and globally uniform (set to its mean equatorial profile). Aerosol effects are not considered.

2.2. Self-Aggregation Behavior

We perform a series of 2 year RCE experiments for SSTs ranging from 290 to 308 K (longer experiments do not exhibit significantly different aggregation characteristics). Each simulation starts from horizontally uniform initial conditions which correspond to the globally averaged temperature, wind, and humidity profiles derived from a previous RCE simulation run at the same prescribed SST but initialized by an atmospheric state corresponding to a SST of 300 K. Note that, at each SST, the global mean state chosen to initialize the 2 year experiments is obtained by averaging a simulation with slightly aggregated convection (to avoid differences in the mean state of the atmosphere due to differences in the state of aggregation [Bretherton *et al.*, 2005; Tobin *et al.*, 2012]).

A white noise of small amplitude is added to the humidity field at 600 hPa to break the symmetry of the initial conditions and let the potential RCE instabilities develop. The type of atmospheric organization that emerges from these experiments at 292 or 307 K is illustrated by two snapshots of the global atmosphere at two different times of the simulation (usually, self-aggregation starts within the first 2 months, with only a few cases starting later). Between day 40 and day 290 at 292 K (Figures 1a and 1c), and between day 400 and day 650 at 307 K (Figures 1b and 1d), the convective organization evolves from a state when convection is randomly distributed across the domain, to the point when a large-scale circulation arises and the atmosphere organizes into large dry areas and narrow areas of strong precipitation. This spontaneous evolution is consistent with a convective self-aggregation behavior taking place at the large-scale. At 292 K, convection aggregates in the form of small isolated clusters or long lines of intense precipitation converging toward an intense convective center. These convective centers move around slowly, but decreasingly so as they become more intense. At 307 K, an even stronger and more localized organization emerges.

Different metrics may be used to characterize convective aggregation quantitatively. The simple convective aggregation index (SCAI) defined by Tobin *et al.* [2012] to characterize the density and the scattering of convective clusters within a $10^\circ \times 10^\circ$ domain using high-resolution satellite observations (0.5° , 6 hourly) is not suited here because of the lack of spatial and temporal resolution of GCM outputs. However, the development of convective aggregation in the GCM is closely associated with the tendency of the atmosphere to develop large areas of dry, subsiding air, and the tendency of convection to clump within narrow areas of large-scale ascents. It is closely associated with the emergence and strengthening of a large-scale overturning circulation, whose strength can be characterized by the statistical distribution over the globe of mid-tropospheric (500 hPa) large-scale vertical velocities. As long as convection remains randomly distributed within the domain, the large-scale ascents and descents are weak and cover approximately the same area. In contrast, as soon as convective aggregation develops, the strength of large-scale ascents increases. Owing to mass conservation and the fact that vertical velocity in subsidence areas is constrained by the rate of clear-sky radiative cooling and static stability, it is associated with an expansion of the area covered by large-scale subsidence. In the following, we thus characterize the degree of aggregation of convection in the GCM by the fractional area of the globe covered by large-scale subsidence in the mid-troposphere, a quantity that we will refer to as the subsiding fraction (SF). SF is close to 0.5 when convection is disaggregated, but it can reach much higher values when convection is aggregated (Figure 1e).

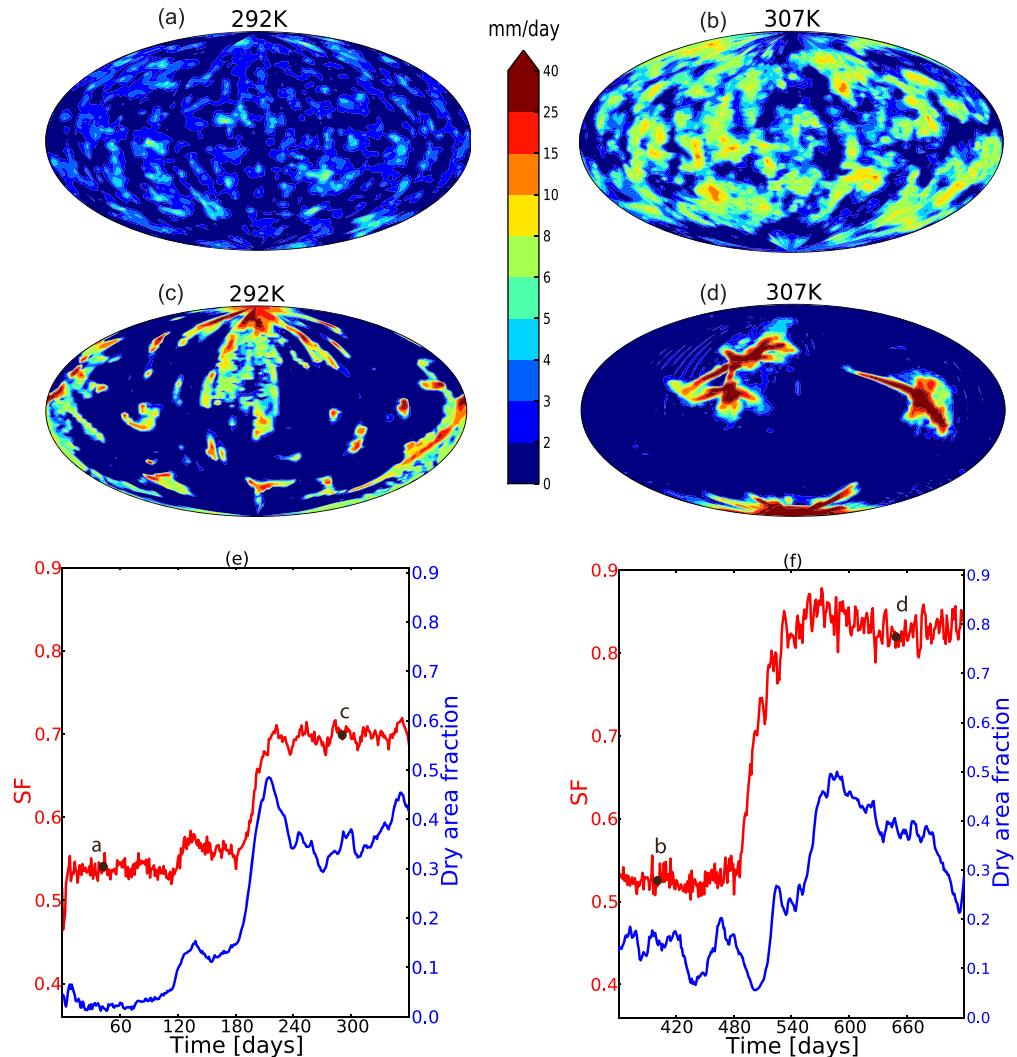


Figure 1. Global snapshots of precipitation for disaggregated convection at (a) day 40 at 292 K and (b) day 400 at 307 K, and for aggregated convection at the same SSTs (respectively, (c) at day 290 and (d) at day 650). Temporal evolution of subsiding fraction (SF, red) and proportion of dry areas (blue) for the reference simulations at (e) 292 K and (f) 307 K. The approximate timing of the snapshots shown on Figures 1a–1d is reported on Figures 1e and 1f.

2.3. Sensitivity to SST and Initial Conditions

The SF index is diagnosed in RCE experiments initialized from horizontally uniform conditions and forced by a range of prescribed SSTs. Three different behaviors can be distinguished depending on SST (red circles in Figure 2). For SSTs lower than 294 K or higher than 305 K, convection self-aggregates and behaves like discussed previously for 292 and 307 K (these two examples are actually representative of what happens for these two ranges of SSTs, respectively). For the large range of intermediate SSTs (294–305 K), the occurrence of self-aggregation is less systematic and depends on initial conditions.

Whatever the initial conditions, self-aggregation is always initiated and maintained at SSTs lower than 294 K or higher than 305 K (pink triangles in Figure 2). By contrast, for SSTs in the range 294–305 K, even if most cases show a triggering of self-aggregation, in many simulations, self-aggregation cannot be maintained. For most SSTs, initializing the simulation with an aggregated state is enough to develop and/or maintain aggregation (black circles in Figure 2). As in CRMs [Khairoutdinov and Emanuel, 2010; Muller and Held, 2012; Muller and Bony, 2015], the atmosphere simulated by the GCM thus exhibits a strong hysteresis behavior. Around 299–300 K, however, whenever convection starts aggregating, it disaggregates progressively after a few days, suggesting that convection is reluctant to maintain a state of self-aggregation at these surface

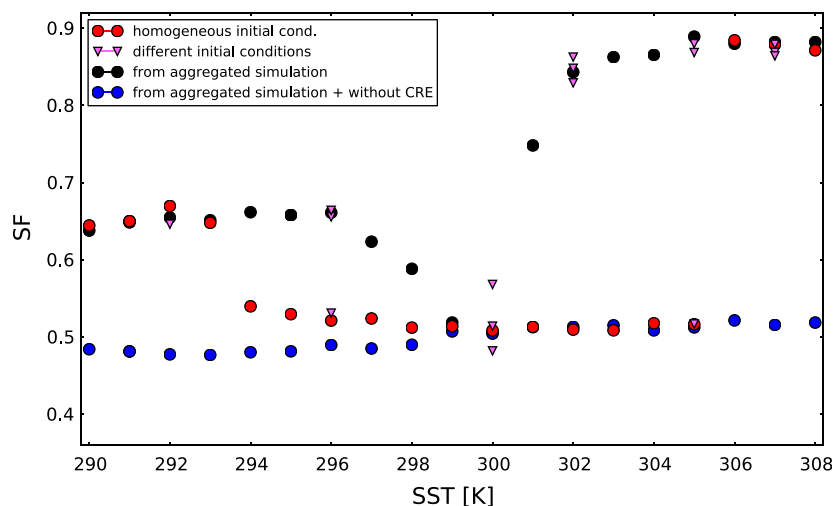


Figure 2. Subsidence fraction (SF) at equilibrium (mean over the last 6 months) for SST ranging from 290 to 308 K. Red circles correspond to simulations starting with homogeneous conditions (mean humidity, temperature, and wind vertical profiles imposed with white noise for humidity at 600 hPa) of RCE simulations at the same slightly aggregated state and same SST. Pink triangles start from the same simulations with different variables homogenized (either wind, or humidity, or both). Black and dark blue circles start from an aggregated simulation, with or without cloud-radiative effects (CRE) during the simulation.

temperatures. Note that cloud-radiative effects are responsible for the maintenance of self-aggregation, as aggregated simulations run without cloud-radiative effects systematically become disaggregated (blue circles in Figure 2).

In summary, the organization of convection exhibits two different regimes depending on SST. At low and high SSTs, RCE instability always occurs and self-aggregation always develops, irrespective of initial conditions. At intermediate SSTs, the occurrence of self-aggregation is sensitive to initial conditions, and its triggering does not necessarily imply its subsequent maintenance. In the rest of the study, we unravel the physical processes responsible for the triggering of self-aggregation in these different ranges of SST.

3. Moist Static Energy Budget

3.1. Analysis Framework

Following Bretherton *et al.* [2005], Muller and Held [2012], and Wing and Emanuel [2014], we analyze the moist static energy (MSE, noted h) defined as:

$$h = c_p T + gz + L_v q_v \tag{1}$$

where c_p denotes the specific heat of dry air, T the temperature, gz the geopotential, L_v the latent heat of vaporization, and q_v the water vapor mixing ratio.

To investigate the physical processes leading to self-aggregation, we analyze the daily budget of vertically integrated moist static energy, \hat{h} , and look at the different sources and sinks of MSE:

$$\frac{\partial \hat{h}}{\partial t} = F_s + \text{NetSW} + \text{NetLW} + \text{Adv} \tag{2}$$

with F_s being the surface enthalpy flux defined as the sum of latent and sensible heat fluxes (LHF and SHF, respectively), NetSW and NetLW the column SW and LW radiative flux convergences, respectively, and $\text{Adv} = -\nabla_h \cdot \hat{u} \hat{h}$ the horizontal divergence of the density-weighted vertical integral of the MSE flux. This advective term is calculated as a residual from the rest of the budget. Following Wing and Emanuel [2014], the feedbacks affecting self-aggregation are elucidated through the budget analysis of the spatial variance of MSE:

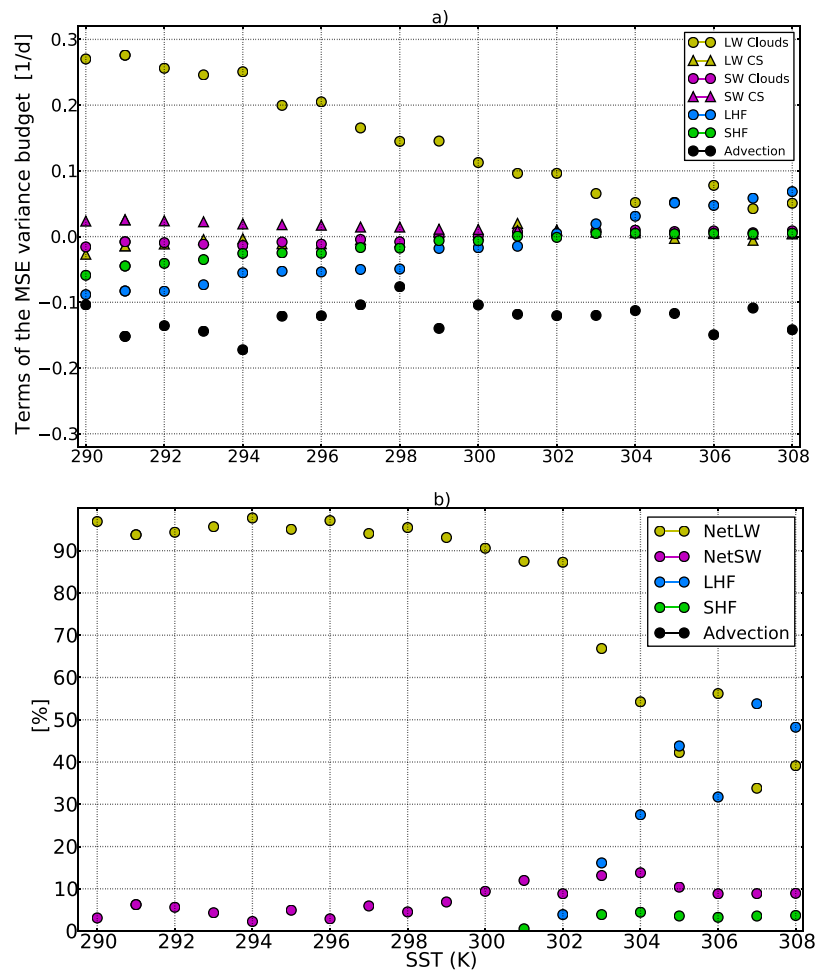


Figure 3. (a) LW (yellow) and SW (pink) due to clouds (circles) or clear sky (triangles), LHF (blue), SHF (green), and advection (black) covariance terms of equation (3) for SSTs between 290 and 308 K. Shown are averages for the initiation period. (b) Relative proportion of positive feedbacks on self-aggregation as a function of SST over the same period. NetLW and NetSW correspond to the total (clear sky and clouds) LW and SW terms.

$$\frac{1}{2} \frac{\partial \hat{h}^2}{\partial t} = \hat{h}' F_s' + \hat{h}' \text{NetSW}' + \hat{h}' \text{NetLW}' + \hat{h}' \text{Adv}' \quad (3)$$

where primed terms (.)' correspond to anomalies from the global mean of the daily outputs. Each term on the right-hand side of the equation represents the covariance between MSE sources and MSE anomalies, and, if positive, indicates a positive feedback on self-aggregation.

3.2. Temperature Dependence of the Feedbacks

To determine which feedbacks are active when the initiation of self-aggregation starts, we look for a clear transition from a disaggregated state to an aggregated one. For this purpose, we identify in simulations the moment (after spin-up) when SF rapidly increases from a value of about 0.5 to its maximum value. Examples of such transitions are shown in Figures 1e and 1f, close to day 190 and 480, respectively. For each simulation, we then define the initiation period as the period starting 15 days before the initiation date and ending 10 days after, so as to encompass what happens before the initiation and shortly after.

The analysis of the MSE variance budget for a range of SSTs shows that the feedbacks controlling the initiation of self-aggregation vary with SST (Figure 3a). At all SSTs, the radiative feedbacks are positive and the LW feedback largely dominates, although it weakens as SST increases. In comparison, the SW feedback is very small and nearly constant. The positive LW feedback is almost entirely due to clouds, while the SW feedback is mainly due to clear-sky effects. For SSTs less than 302 K, the LW feedback is the main feedback

governing the initiation of self-aggregation (representing about 90% of the positive covariance term in Figure 3b). The advective term is always negative. Beside the LW feedback, the covariance terms exhibiting the largest dependence on SST are those associated with the sensible and latent heat fluxes: the LHF term increases substantially with SST and above 302 K, its contribution to the MSE variance becomes positive and of similar magnitude as that of the LW feedback (Figure 3b). The SHF contribution is negative at low SSTs but becomes positive above 300 K and then stabilizes at a value close to that of the SW feedback.

To interpret the temperature dependence of convective self-aggregation, we study below the physical mechanisms underlying these feedbacks. We first consider the case of low and high SSTs (considering the representative cases of 292 and 307 K), and then the case of intermediate SSTs.

4. Mechanisms Triggering Self-Aggregation at Low Sea Surface Temperature

4.1. Phenomenology

To examine the triggering of self-aggregation at 292 K, we analyze the simulation initialized with horizontally homogeneous conditions of wind, humidity, and temperature (Figure 1, left column). This simulation presents two distinct phases on its way toward aggregation: from day 120 to day 190, SF is fairly constant (close to about 0.55), while after day 190, it suddenly increases before reaching a new equilibrium value of about 0.7 (Figure 1e). A visual inspection of the simulation shows that the triggering is preceded by the rapid expansion and strengthening of dry and cold patches devoid of deep convection (dry areas are defined by a threshold at 15 kg m^{-2} on precipitable water). To understand the mechanisms underlying the triggering of convection around day 190, we focus on a region of about $80^\circ \times 140^\circ$ containing one of these cold patches. It appears around day 120 and subsequently expands (see Figure 1e for the time evolution of the area covered by cold/dry patches, and Figure 4 for the appearance and growth of the patches). A second patch develops in parallel in the Southern Hemisphere after day 120. These patches are associated with a strong subsidence in the mid-troposphere, the presence of low clouds in the planetary boundary layer, strong gradients of temperature and humidity at their borders, and a divergence of the near-surface wind (Figure 4).

The different cold/dry patches of the domain expand and get closer to each other until they connect. Their merging coincides with an abrupt expansion of the area covered by dry regions over the globe and a large increase of SF (Figure 1e). The initiation of self-aggregation thus appears to be related to the expansion of cold/dry patches that progressively isolate deep convection and force the clumping of convective clouds away from these patches.

4.2. Radiatively Driven Cold Pools

The behavior of cold patches in this simulation at 292 K is reminiscent of density currents that occur in the atmosphere when air masses of different densities come in contact, with the denser air sinking down and spreading out along the surface. In convective situations, such density currents occur for instance when convective downdrafts generated by the evaporation of rain forms a pool of cold air in the boundary layer which is denser than its surrounding environment and spreads out horizontally near the surface. The velocity at which the cold pool spreads out (C_{*} , defined here as the 10 m wind speed averaged over the surface of the cold pool) depends on the virtual potential temperature difference between the cold pool and its environment, as expressed by the potential energy E_p [Rotunno *et al.*, 1988; Grandpeix and Lafore, 2009]:

$$E_p = -g \int_0^{h_{bl}} \frac{\overline{T_{vp}} - \overline{T_{ve}}}{\overline{T_{ve}}} dz \quad (4)$$

where h_{bl} is the height of the boundary layer (determined by eye), and $\overline{T_{vp}}$ and $\overline{T_{ve}}$ the mean virtual temperatures within and outside the cold pool, respectively. Using the hydrostatic equilibrium equation, and assuming that $\overline{T_{ve}} = \overline{T_v}$, (4) can be written as

$$E_p = R \int_{P_{bl}}^{P_{surf}} (\overline{T_{vp}} - \overline{T_v}) \frac{dP}{P} \quad (5)$$

where P_{bl} is the pressure at the top of the boundary layer and P_{surf} , the surface pressure.

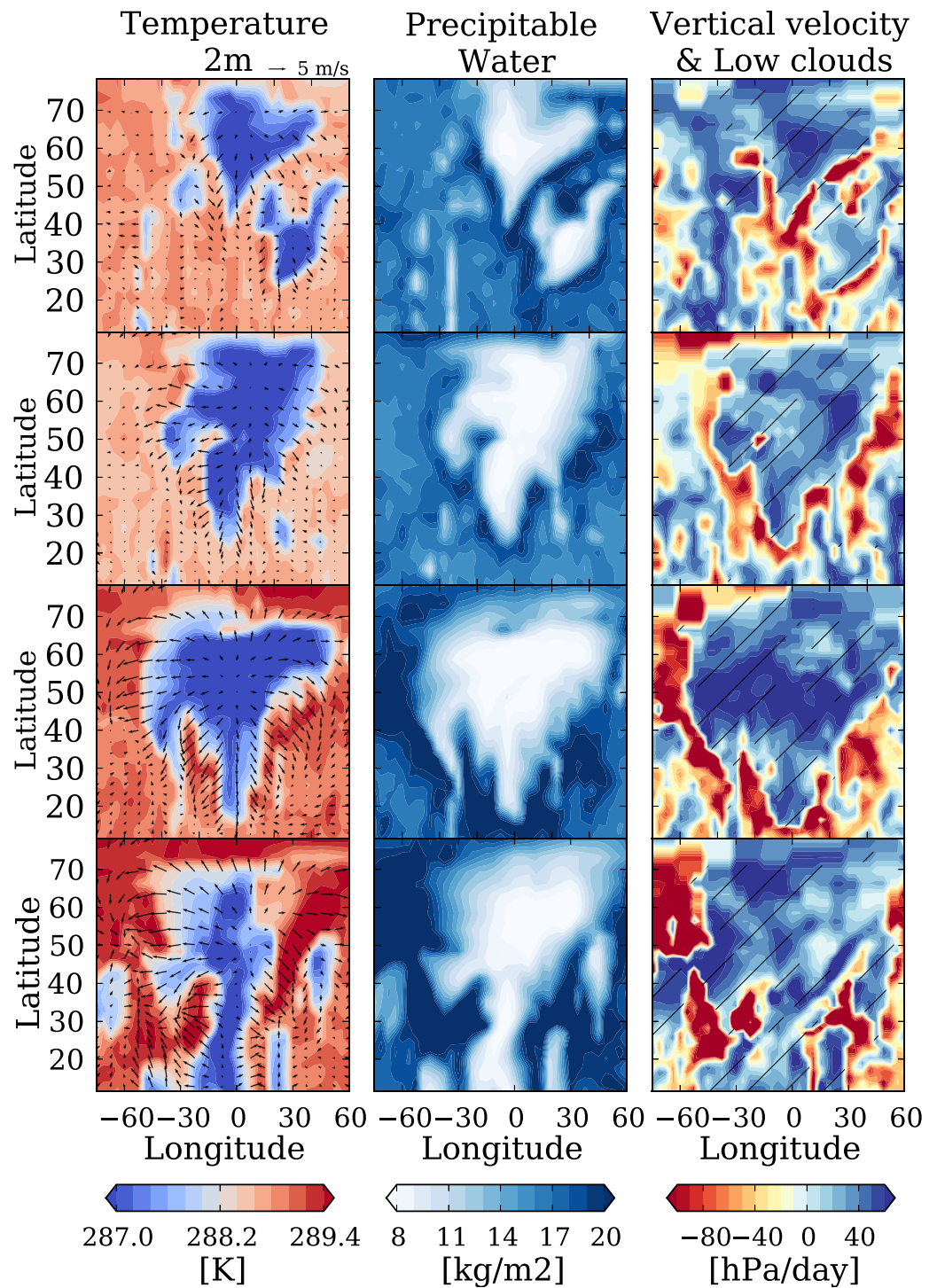


Figure 4. Zoom on a large region of the planet ($80^\circ \times 140^\circ$) showing a cold/dry pool in the reference simulation at 292 K. Each row is a snapshot at a (first row) day 125, 151, 177, and (fourth row) 193. First column shows temperature at 2m (shading) and wind at 10 m (arrows). Second column represents precipitable water and the third one the vertical velocity at 500 hPa (shading, negative upward) and low-level cloud cover >50% (hatchings).

To investigate the extent to which the spreading of the dry, cold patches in our simulations can be interpreted as the behavior of a density current, we use equation (4) to estimate the potential energy associated with the cold patches, and examine the relationship between the velocity at which the patches spread out and the square root of their potential energy. Following *Grandpeix and Lafore* [2009], we relate both quantities using

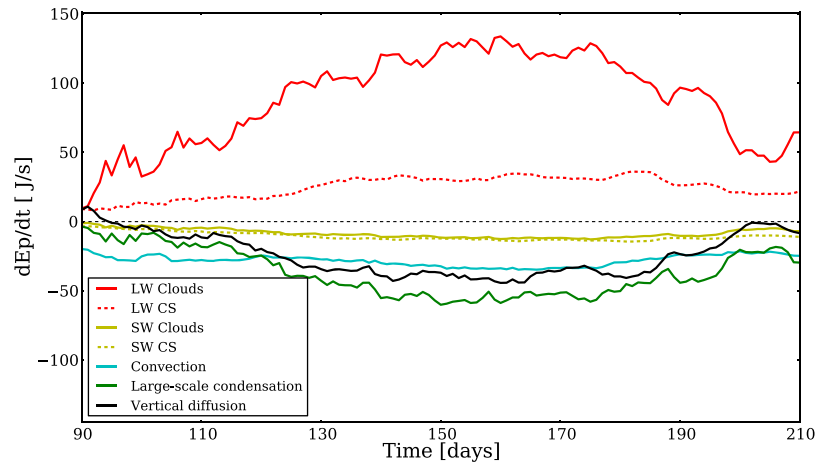


Figure 5. Temporal evolution of the different terms of equation (7) over the same region as in Figure 4: LW due to clouds (red) and clear sky (red dashed), SW due to clouds (yellow) and clear sky (yellow dashed), convection (blue), large-scale (green) and boundary layer (black).

$$C_* = k_* \sqrt{2E_p}$$

where k_* is a positive parameter. In our simulations, C_* values (that range from 1 to 4 $m s^{-1}$) and E_p values (that range from 7 to 30 J) are actually well correlated ($R = 0.90$), with $k_* = 0.42$ (the methods used to compute C_* slightly affect k_* but do not change the correlation with E_p). This value is close to that estimated for squall lines based on 2D simulations (0.68 in Lafore and Moncrieff [1989]), 3-D simulations (0.33 in J.-P. Lafore (personal communication, 2000)), or observations (0.5 in Bryan *et al.* [2005]). It suggests that the behavior of cold patches in our simulations can actually be interpreted as cold pools, whose origin is not the reevaporation of rain like in convective cases, but another mechanism to be explained.

For this purpose, we diagnose the influence of physical processes on T_v and then on the building of E_p . If $\left(\frac{dT}{dt}\right)_i$ and $\left(\frac{dq}{dt}\right)_i$ are the tendencies of process i on temperature and humidity, respectively, then

$$\sum_i \left(\frac{dT_v}{dt}\right)_i = \sum_i \left[(1 + \epsilon q) \left(\frac{\partial T}{\partial t}\right)_i + \epsilon T \left(\frac{\partial q}{\partial t}\right)_i \right] \quad (6)$$

Assuming that $\frac{dp}{p}$ does not vary over time (which is true at first order), using (6) and $\Delta \overline{T}_v = \overline{T}_e - \overline{T}_{vp}$, equation (5) becomes:

$$\frac{dE_p}{dt} = \sum_i \left[R \int_{P_{surf}}^{P_{bl}} \frac{dP}{P} \left(\frac{\partial \Delta \overline{T}_v}{\partial t}\right)_i \right] \quad (7)$$

with, at first order,

$$\left(\frac{\partial \Delta \overline{T}_v}{\partial t}\right)_i = (1 + \epsilon \overline{q}_e) \left(\frac{\partial \overline{T}_e}{\partial t}\right)_i + \epsilon \overline{T}_e \left(\frac{\partial \overline{q}_e}{\partial t}\right)_i - (1 + \epsilon \overline{q}_p) \left(\frac{\partial \overline{T}_p}{\partial t}\right)_i - \epsilon \overline{T}_p \left(\frac{\partial \overline{q}_p}{\partial t}\right)_i \quad (8)$$

and \overline{T}_p , \overline{q}_p , \overline{T}_e , \overline{q}_e being the mean temperature and mean specific humidity inside and outside the patch, respectively. Index i corresponds to each term that affects the temperature and humidity budgets, namely LW and SW radiation, convection, large-scale condensation, and vertical diffusion. This enables us to identify and quantify the processes that tend to increase $\frac{dE_p}{dt}$ and thus contribute to the expansion of the cold pools. This analysis is applied to the boundary layer of the zoomed-in region shown in Figure 4, but the results are qualitatively similar when it is applied to the whole globe (not shown). The patches are defined as the regions where the precipitable water is smaller than 15 kg/m^2 (the result is not sensitive to this threshold as long as we keep it under 18 kg/m^2 , not shown).

Figure 5 shows that the large LW radiative cooling of the cold pools relative to their environment is the primary contributor to E_p and thus to the spreading of the cold pools. All other processes exert negative influences on the development and maintenance of E_p . The strong LW atmospheric cooling is primarily due to

the presence of low-level clouds (which can exert local LW coolings as high as tens of K/day) and, to a lesser extent, to the strong clear-sky radiative cooling of the boundary layer in the presence of large-scale subsidence and dry conditions in the free troposphere aloft. By cooling the cold/dry patches (i.e., low-MSE areas), low-level clouds contribute to enhance the MSE variance of the domain, and thus contribute to the strong LW feedback noticed at low SSTs in Figure 3 (note that the different sign of the clear-sky LW and SW feedbacks between Figures 3 and 5 is related to the fact that feedbacks in Figure 5 are integrated over the whole troposphere while E_P is integrated over the boundary layer only).

This analysis thus suggests that the formation and expansion of cold pools in our simulations results from the interplay between low clouds, radiation, and circulation. Since the formation of cold pools is driven by radiative effects (as opposed for instance to the reevaporation of rain in convective situations), we will refer to them as “radiatively driven” cold pools.

4.3. Cloud-Radiative Effects and Shallow Circulation

To explore further the role of cloud-radiative effects in the triggering of self-aggregation, we design mechanism-denial experiments: we restart a simulation at day 90 and switch off the radiative effects of clouds in the lower and/or upper troposphere. When boundary layer clouds are made transparent to radiation, convective self-aggregation never happens (red line in Figure 6a), supporting the idea that low clouds actually play a critical role in the initiation of self-aggregation. However, switching off the radiative effects of free tropospheric (above the 700 mb level) clouds also prevents self-aggregation from happening (blue line in Figure 6a), indicating that high-cloud radiative effects are also needed.

To better understand the role of low clouds and high clouds in the initiation of self-aggregation, we follow Bretherton *et al.* [2005] and analyze the effective stream function Ψ :

$$\Psi_i(z) = \Psi_{i-1}(z) + w_i(z)\bar{\rho}(z) \quad (9)$$

(with $\Psi_0(z) = 0$ for all z , w the vertical velocity and $\rho(z)$ the mean density profile) in a height-CRH space (CRH is the column relative humidity). Ψ provides us with a simple visualization of the main circulations that develop within the domain, and helps understand how MSE is exchanged between dry and moist areas. The analysis is applied to the area (considered in Figure 4) that encompasses a large cold pool and its surroundings, but similar results are obtained when considering the global domain (not shown).

In the presence of low-cloud radiative effects (Figures 6b–6d), a horizontal MSE gradient develops within the first 3 km of the atmosphere and a shallow overturning circulation builds up (as seen on Figures 6c and 6d by the shift and narrowing of the Ψ contours close to the ground and the development of a secondary maximum below 5 km). As shown by Figure 7, this circulation mainly decreases \hat{h} in the moist regions and increases it in the dry ones, leading to a negative feedback of the vertically integrated advective term ($\hat{h}' Adv'$ in equation (3)) almost everywhere. In Figure 6e, the circulation at day 220 resembles the circulation before self-aggregation and does not exhibit any low-level circulation, showing that low-cloud radiative effects play an active role in the development of the shallow circulation. By enhancing subsidence/drying in low-MSE regions and convergence/moistening in moist regions, the shallow circulation promotes the development of convective aggregation. Moreover, Figure 6f shows that in the absence of cloud-radiative effects in the free troposphere, the atmospheric circulation is nearly suppressed, showing that high-cloud radiative effects are necessary to the occurrence of large-scale overturning circulations.

The physical mechanism underlying the initiation of self-aggregation at low SSTs can thus be summarized as follows: (random) events of large-scale subsidence which are strong enough to favor the formation of low-level clouds and to dry the free troposphere aloft, induce an intense radiative cooling of the boundary layer. This cooling leads to the formation of radiatively driven cold pools which expand like density currents, and initiate the aggregation of convection outside of these cold pools. In parallel, cold pools enhance large-scale subsidence and low-level outflow in the lower troposphere, which contributes to the development of a shallow overturning circulation between dry and moist regions. This shallow circulation is further promoted by the remote high-cloud radiative effects. By promoting the maintenance of large-scale subsidence and low clouds, this low-level circulation amplifies the mechanism that gave rise to the expanding cold pools and further forces the convection to aggregate in high-MSE areas at the edge or in-between cold pools.

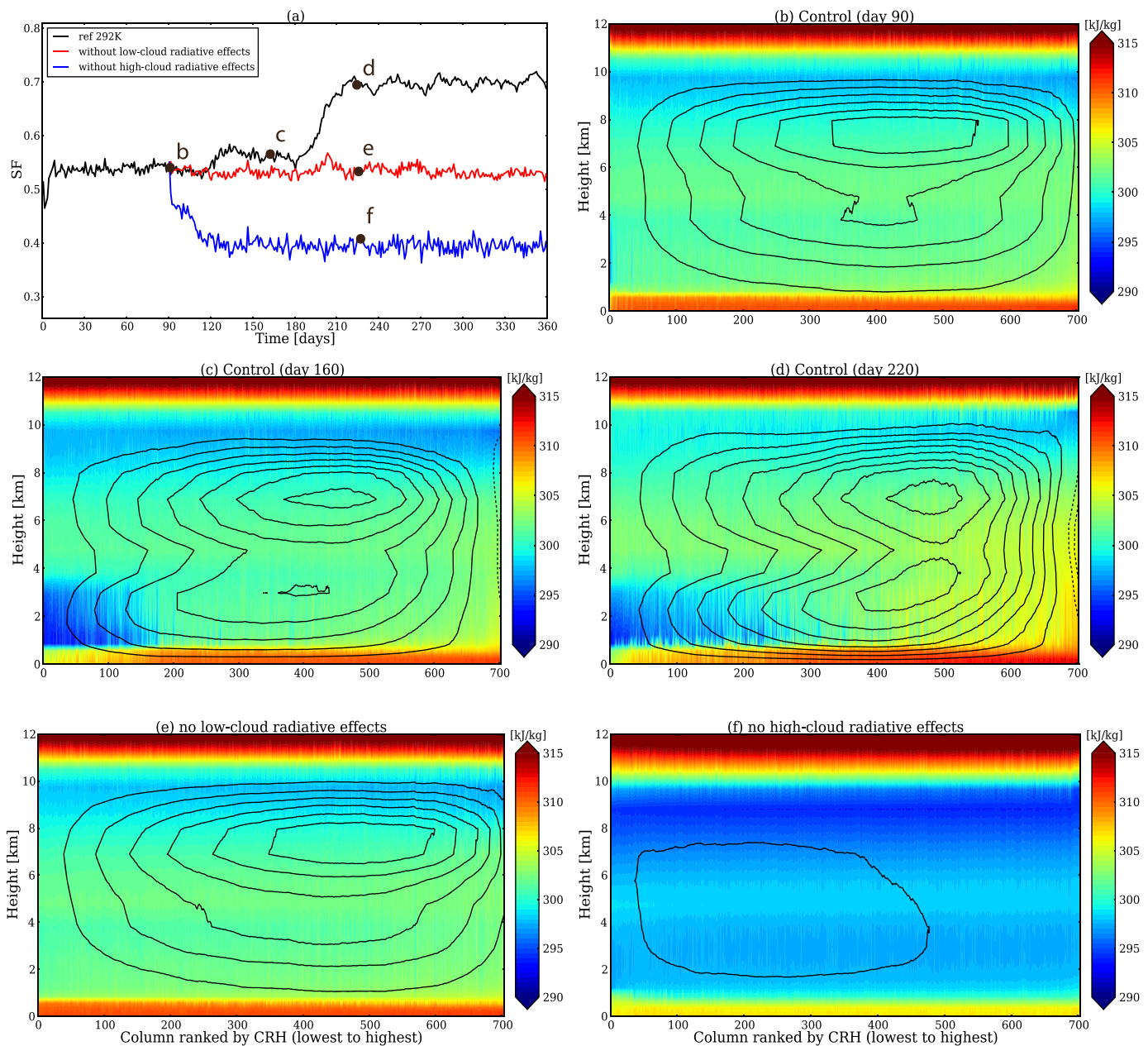


Figure 6. (a) Temporal evolution of SF for the reference simulation (black) and, starting from the same conditions at day 90, for the simulation without radiative effects of low clouds (red) or without radiative effects of high clouds (blue). (b–d) Daily mean circulation for the reference simulation at day 90, 160, and 220, respectively. (e and f) Daily mean circulation at day 220 for the simulations without low-cloud radiative effects and without high-cloud radiative effects, respectively. Black contours represent the stream function Ψ (contours interval = $0.5 \text{ kg m}^{-2} \text{ s}^{-1}$ starting at $0.5 \text{ kg m}^{-2} \text{ s}^{-1}$, dashed if negative). Shading corresponds to moist static energy. On the x axis, dry regions are on the left and moist regions on the right, sorted according to column relative humidity (CRH).

5. Mechanisms Triggering Self-Aggregation at High SST

5.1. Phenomenology

To study the triggering of self-aggregation at high SSTs, we analyze a simulation forced by a SST of 307 K and starting from horizontally homogeneous wind, humidity, and temperature conditions. This SST is representative of the range of SSTs ($>305 \text{ K}$) for which the self-aggregation always triggers whatever the initial conditions. At the beginning of the simulation, convection is randomly distributed over the globe (Figure 1b). However, as soon as an area of deep convection develops in one point of the planet (here close to 59°N and -120°E , Figure 8, first row on the left), it remains localized and expands, giving rise to a self-

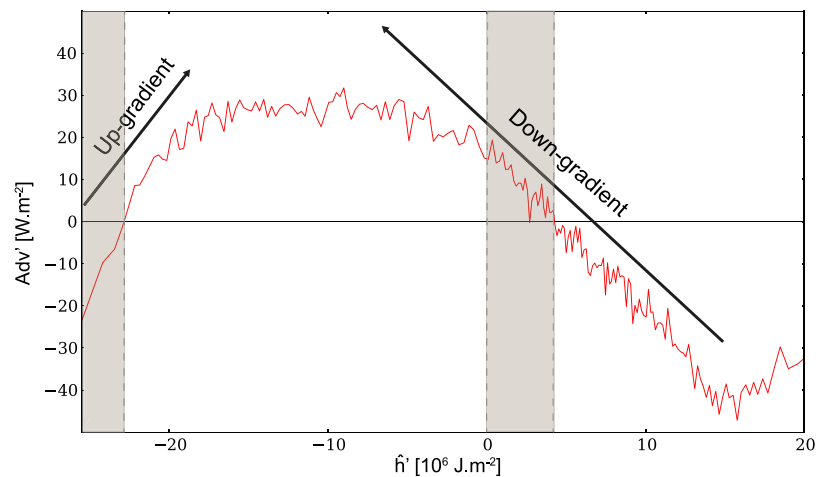


Figure 7. Advection anomaly (Adv') as a function of \hat{h}' calculated over the same region as in Figure 4 during the initiation period. Both terms are integrated over the troposphere. Grey shading indicates a positive feedback of $\hat{h}' Adv'$ (equation (3)) while areas without shading indicate $\hat{h}' Adv' < 0$, showing the dominance of the negative feedback. Dry regions correspond to $\hat{h}' < 0$ and moist regions to $\hat{h}' > 0$.

aggregation of deep convection (Figure 8, middle and right columns). Note that unlike in Held *et al.* [2007], more than 90% of the precipitation is convective in that point, which means that it is not a grid point storm.

A few days before the initiation (at day 480) of convective self-aggregation, the surface wind field starts converging toward the convective area and new convective cells develop in the vicinity of the previous convective cluster (Figure 8, third row). Once self-aggregation is initiated (Figure 8, last row), the lower-tropospheric convergence of winds strengthens and covers an increasingly large domain, and new convective cells develop on the edges of previous convection.

5.2. Role of Cloud Radiative Effects

One striking difference between initiation at 292 and 307 K is the absence of low clouds in the initiation area (no hatchings in Figure 8), suggesting that low-level clouds do not play any role in the triggering of self-aggregation at high SSTs. This is confirmed by a simulation performed without low-cloud radiative effects, which exhibits a self-aggregation behavior similar to that of the control simulation (Figure 9). However, imposing low-cloud radiative effects in the dry regions of a disaggregated simulation (using a radiative heating profile comparable to that found in low-cloud regions at lower SSTs) is enough to force the occurrence of self-aggregation (not shown). It suggests that the reason why low-level clouds do not play an important role here is that the low-cloud amount is too small at high SSTs (the strong decrease of the low-cloud amount as SST rises is a well-known feature of this model [Brient and Bony, 2012; Vial *et al.*, 2013]) to produce a significant radiative cooling of the boundary layer. Cloud radiative effects in the free troposphere, on the other hand, appear to be necessary for the initiation of self-aggregation (Figure 9): by reducing the atmospheric radiative cooling, they increase the net input of energy into the column and favor the development of large-scale ascents as soon as convection and clouds reach the free troposphere, i.e., as deep convection develops in the vicinity of existing convection. Furthermore, as high clouds occur in moist regions, their radiative effects contribute to the LW radiative feedback discussed in section 3.2 and thus enhance the spatial variance of MSE (equation (3)).

5.3. Role of WISHE

We identify high clouds as an important contributor to the initiation of self-aggregation. However, as discussed earlier, the period before initiation is characterized by major changes in the surface wind field. We hypothesize that the mass convergence associated with the convective cluster leads to an increase of the surface winds, and then of surface fluxes, in surrounding areas. By increasing the moist entropy of the sub-cloud layer, enhanced surface fluxes are likely to favor the development of convection in the vicinity of the existing cluster, and thus to promote the expansion of the convective area. To test this hypothesis, we run a simulation at 307 K starting at day 450 of the reference simulation, and impose an homogeneous wind in the calculation of surface turbulent fluxes. When the surface wind anomalies are not coupled to surface

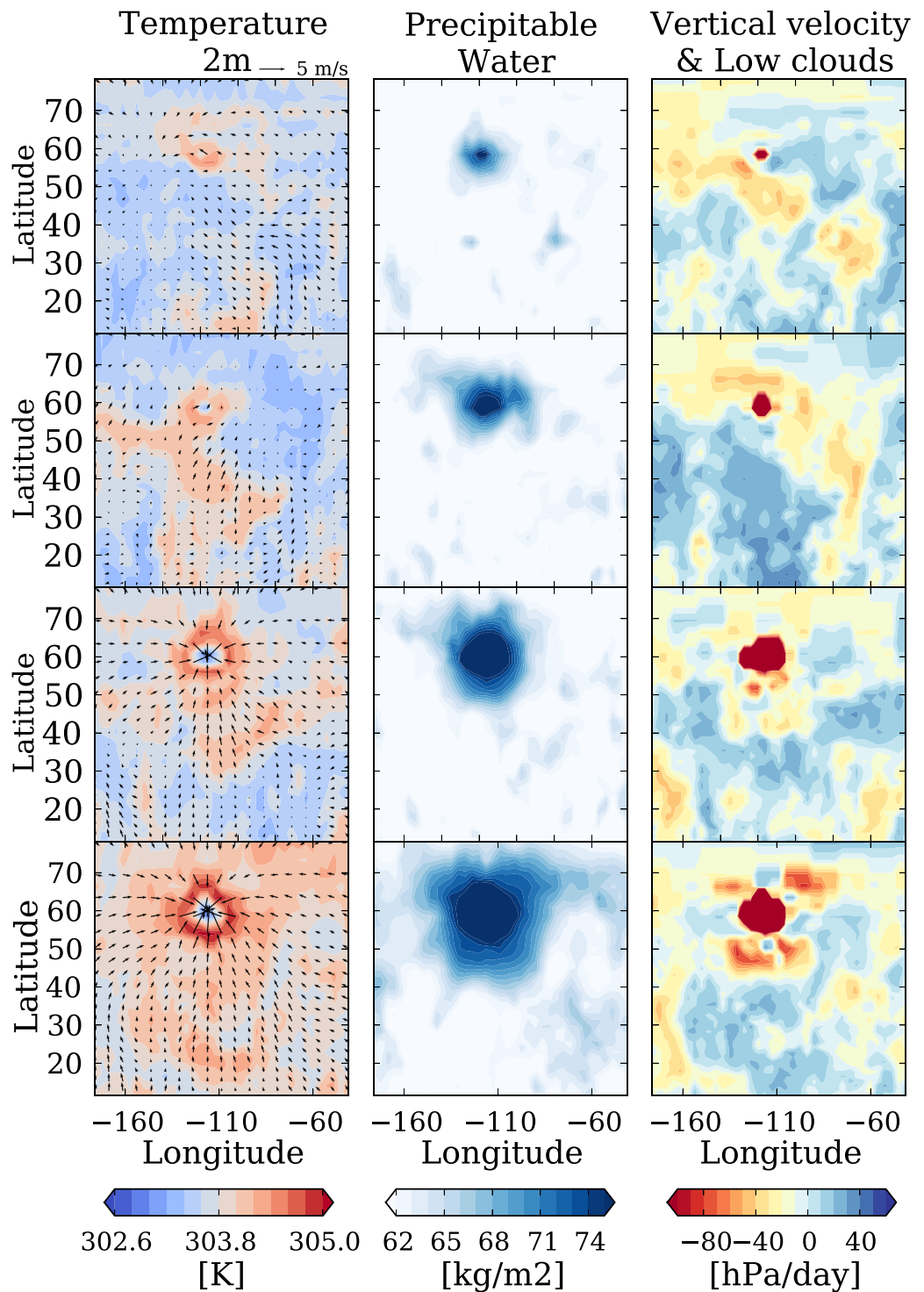


Figure 8. Same as Figure 4 but for a $80^\circ \times 140^\circ$ region in the reference simulation at 307 K showing the area from where aggregation starts. Each row is a snapshot at a day (first row) 468, 473, 478, and (last row) 483.

fluxes, no self-aggregation arises (Figure 9). It supports our hypothesis and shows that self-aggregation is triggered by the wind-induced surface heat exchange (WISHE) feedback [Emanuel, 1987; Neelin et al., 1987].

These experiments highlight the role of two critical mechanisms in the initiation of self-aggregation, one related to surface fluxes (F_s) and the other one to the atmospheric radiative cooling ($Q_{rad} = \text{NetLW} + \text{NetSW}$). To determine whether one acts prior to the other, we examine the time evolution of both

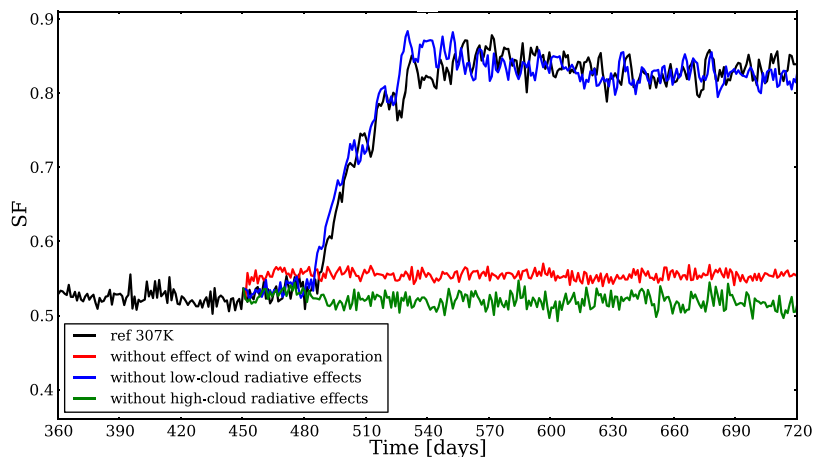


Figure 9. Temporal evolution of SF for the reference simulation at 307 K (black) and, starting from the same conditions at day 450, for the simulation without effect of wind on surface fluxes (red), without low-cloud radiative effects (blue), or without high-cloud radiative effects (green).

variables during the initiation period (Figure 10) over the $80^\circ \times 140^\circ$ domain (the results are qualitatively similar when looking at the whole globe): F_s starts increasing prior to Q_{rad} , in coincidence with the increase (and direction shift) of the surface wind speed (Figure 8). Both terms then increase until the convective cluster disaggregates while other clusters develop elsewhere on the planet following the same mechanism. The lag between F_s and Q_{rad} thus suggests that WISHE plays a dominant role in the triggering of self-aggregation at high temperature, and that its effect is subsequently amplified and maintained by changes in cloud-radiative effects.

6. Temperature Dependence of Initiation Mechanisms

The previous sections identified two main mechanisms of initiation of self-aggregation: the interaction between low-cloud radiative effects, cold pools and shallow circulation at 292 K, and WISHE at 307 K. In all cases, cloud radiative effects in the free troposphere were also found to play an important role in the growth and maintenance of the self-aggregation. To examine the range of SSTs over which these mechanisms play a role in the triggering of self-aggregation, we rerun the simulations of Figure 3 that were developing self-aggregation, but 30 days before the initiation of self-aggregation, we switch off either the low-cloud radiative effects (i.e., from the surface to 700 hPa), the free-tropospheric cloud radiative effects (at heights above the 700 hPa level), or WISHE.

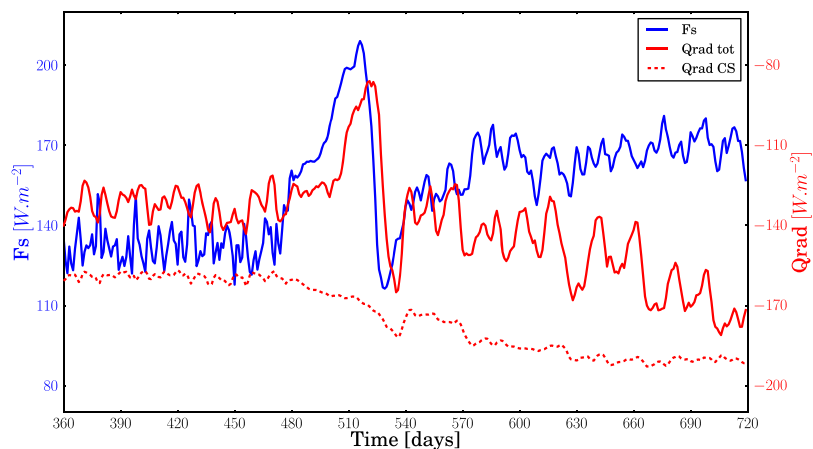


Figure 10. Temporal evolution of the surface enthalpy flux (blue), total and clear sky (CS) radiative (red and red dashed, respectively) terms over the $80^\circ \times 140^\circ$ region for the reference simulation at 307 K.

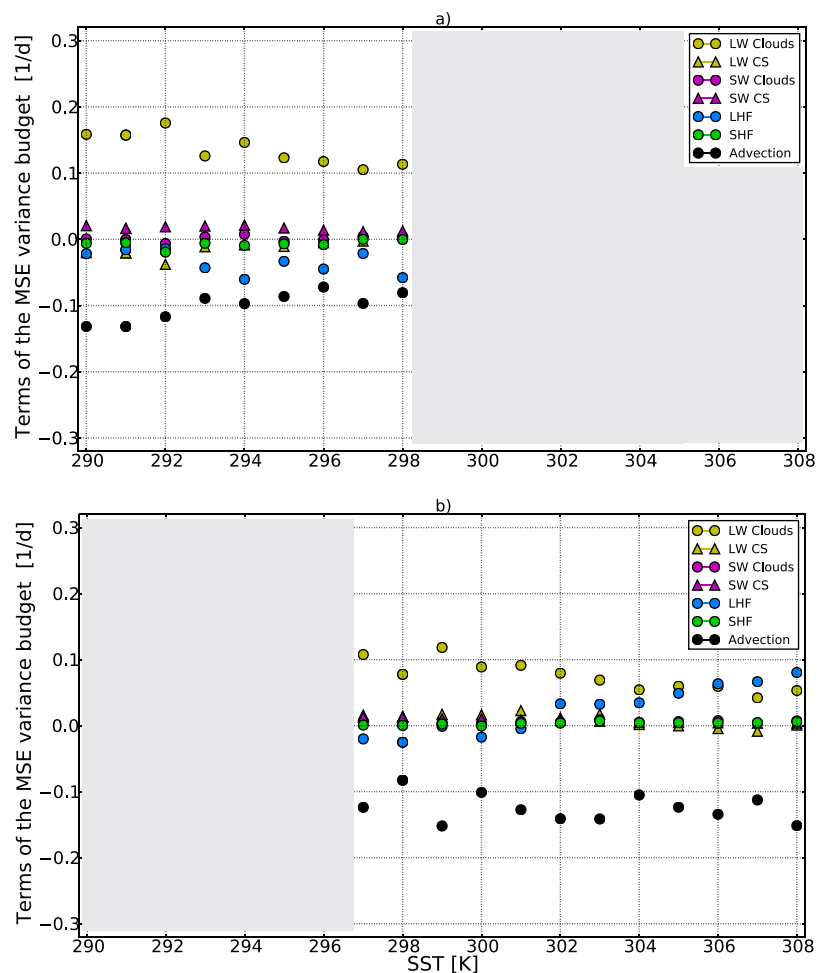


Figure 11. (a) Same as Figure 3a but for simulations without WISHE feedback. (b) Same for simulations without low-cloud radiative effects. Grey spaces correspond to simulations that do not self-aggregate.

When high-cloud radiative effects are switched off, self-aggregation never happens, whatever the SST (not shown). Without WISHE, self-aggregation does not occur anymore at SSTs higher than 298 K, and without low-cloud radiative effects, it does not occur anymore at SSTs lower than 297 K (Figure 11). It suggests that the “radiation-circulation coupling” mechanism discussed in section 4 is necessary to initiate self-aggregation at SSTs lower than 296 K, and that the WISHE mechanism is necessary at SSTs higher than 299 K. At 298 and 299 K, switching off both WISHE and low-cloud radiative effects prevents self-aggregation from occurring (not shown), but switching off only one of these mechanisms does not, suggesting that either mechanism is sufficient to trigger self-aggregation.

Based on this analysis, two questions arise: (i) what explains the temperature dependence of the initiation mechanisms? and (ii) how much do these two mechanisms interact with each other? For a given surface wind anomaly and near-surface relative humidity, the WISHE mechanism is more efficient at high SSTs than at low SSTs because the moisture difference between the surface and the near-surface air just above tends to increase with SST. It likely contributes to make the WISHE mechanism more relevant at high SSTs than low SSTs. In addition, the GCM used in this study is known to produce a strong positive low-cloud feedback as surface temperature rises [Brient and Bony, 2012], i.e., the low-cloud cover decreases strongly as SST rises (in RCE, the model predicts a globally averaged low-cloud cover that decreases from about 40% at 290 K to 7% at 300 K, and 5% at 306 K). It makes the radiative effects of low-level clouds weaker at high SSTs, and therefore the “radiation-circulation coupling” mechanism less efficient. Moreover, the low-cloud radiative effects are known to be strongly coupled to surface turbulent fluxes: by decreasing the MSE of the boundary layer, the LW radiative cooling of low-level clouds

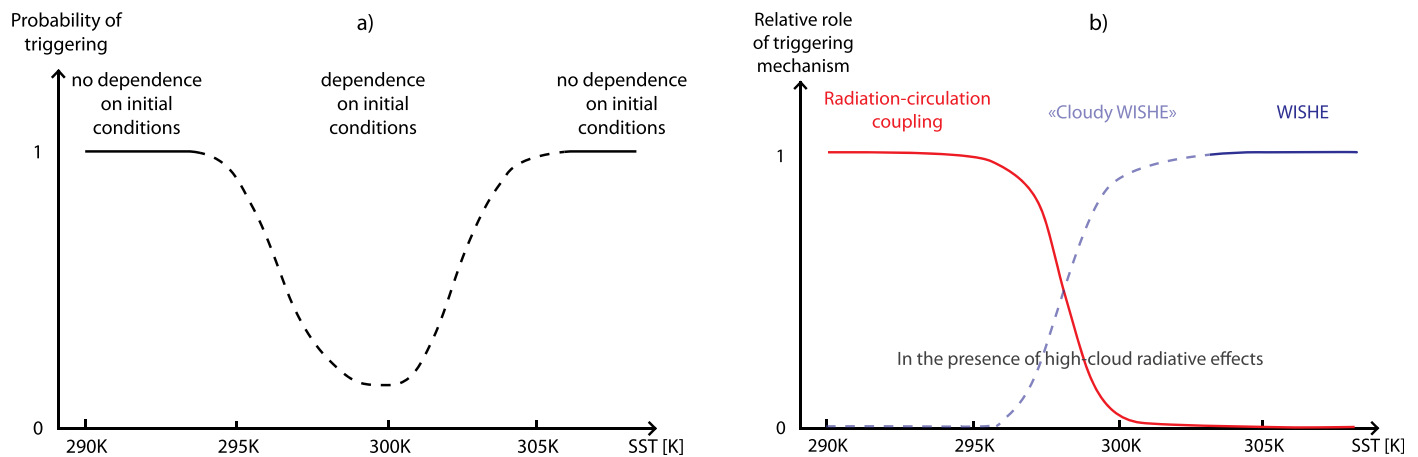


Figure 12. Schematic representation of (a) the probability of triggering self-aggregation as a function of SST and (b) the relative role of the different mechanisms governing self-aggregation depending on SST. The radiation-circulation coupling (red), cloudy-WISHE (dashed blue), and WISHE feedbacks (blue) are represented. Note that self-aggregation can only be triggered if free-tropospheric clouds interact with radiation.

tends to enhance turbulent fluxes at the ocean surface [Fermepin and Bony, 2014; Vial et al., 2015], and the moistening of the boundary layer by surface fluxes has a positive influence on the formation of low-level clouds and thus low-cloud radiative effects [Zhang et al., 2013]. Although the WISHE mechanism can operate in the absence of low-level clouds, the interaction between low-cloud radiative effects and surface fluxes is thus likely to make WISHE more efficient. Therefore, at SSTs for which the low-cloud radiative effects alone are not sufficient to trigger self-aggregation through a “radiation-circulation coupling,” they can still favor the triggering of self-aggregation by making WISHE more efficient. This “cloudy WISHE” is likely at play in our model at SSTs between 295 and 305 K. The influence of low-cloud radiative effects on WISHE also suggests that even in a model that would predict low clouds at high temperatures, the dominant mechanism of self-aggregation could still be WISHE. This is actually confirmed by high-SST experiments in which low-cloud radiative effects are artificially imposed in the simulation (not shown).

7. Summary and Discussion

This study analyses the phenomenon of self-convective aggregation in the IPSL-CM5A-LR GCM run in a non-rotating RCE framework and forced by a range of globally uniform SSTs. As summarized in Figure 12a, self-aggregation is spontaneous at SSTs lower than 294 K or higher than 305 K, whatever the initial conditions. At intermediate SSTs, it is less spontaneous and its occurrence depends on initial conditions. In particular, self-aggregation occurs more easily when initial conditions are derived from a previous experiment in which convection was aggregated. Yet overall self-aggregation tends to occur more easily at low and high temperatures than at intermediate temperatures.

Two main physical mechanisms can trigger self-aggregation in this model, and their relative contribution depends on surface temperature (Figure 12b). At low SSTs, self-aggregation is triggered by a “radiation-circulation coupling”: events of large-scale subsidence which are strong enough to favor the formation of low-level clouds and dry the free troposphere aloft, induce an intense radiative cooling of the boundary layer and the formation of radiatively driven cold pools which expand like density currents. The expansion of the cold pools forces the convection to aggregate at the edges or in-between cold pools (Figure 13a). The development of a shallow circulation between dry and moist regions reinforces subsidence and promotes the formation of low-level clouds in dry regions, which positively contributes to the self-aggregation. At high SSTs, the initiation mechanism is primarily related to the interaction between surface turbulent fluxes and near-surface wind anomalies (WISHE): as deep convection develops somewhere, the mass convergence associated with it enhances the surface wind around the convective area, and then surface fluxes. It promotes the development of deep convection in the vicinity of the existing convection, which eventually yields to convective aggregation (Figure 13b). At intermediate SSTs, self-aggregation is less spontaneous

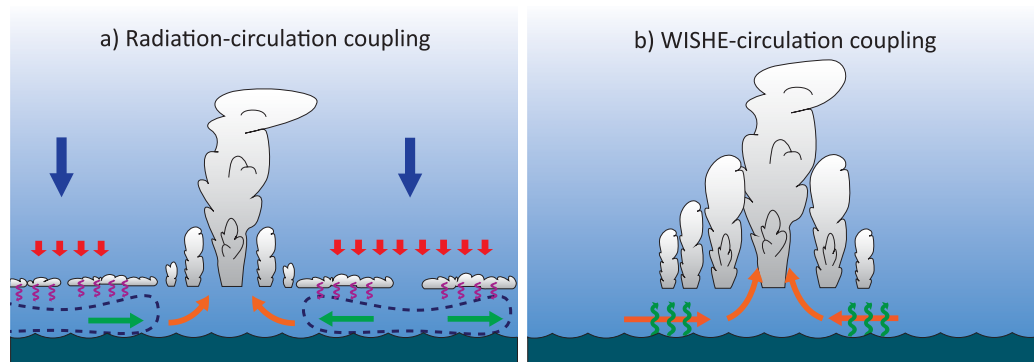


Figure 13. Cartoon illustrating the two main physical mechanisms that initiate self-aggregation in the model. (a) At low SSTs, a strong subsidence promotes the formation of low-level clouds which radiatively cool the lower troposphere, drive the formation of a shallow circulation that increase the subsidence in dry areas, and of “radiatively driven cold pools” that force the convection to aggregate outside of these cold/dry areas. (b) At high SSTs, the development of an isolated convective area is associated with a mass convergence that enhances surface winds and surface turbulent fluxes in the vicinity of existing convection, which favors the triggering of convection in nearby areas and thus convective aggregation.

but it can be triggered by a combination of both mechanisms. At all SSTs, the reduction of the atmospheric radiative cooling by deep convective clouds helps develop a large-scale circulation between dry and moist regions which is necessary to the growth and maintenance of convective aggregation.

The strong temperature dependence of self-aggregation in this model is partly due to thermodynamics (e.g., the higher efficiency of WISHE at high temperatures due to the increase of the surface thermodynamic disequilibrium), and partly due to the strong dependence of low-level clouds on surface temperature. As SST increases, the model predicts a decrease of the low-level cloudiness, and hence makes the formation of radiatively driven cold pools less likely. On the other hand, the coupling between surface fluxes and low-cloud radiative effects makes WISHE more likely to trigger convection at intermediate SSTs (cloudy WISHE). In this model, self-aggregation is least likely to occur around 300 K. It presumably arises from the fact that 300 K is a surface temperature too high for the model to predict a significant low-cloud fraction and therefore an efficient radiation-circulation coupling mechanism, but too low for WISHE to be thermodynamically efficient (especially in the near absence of low-level clouds).

This study thus shows that the phenomenon of self-aggregation pointed out in CRMs [Bretherton *et al.*, 2005; Held *et al.*, 2007; Muller and Held, 2012; Wing and Emanuel, 2014; Wing and Cronin, 2015; Muller and Bony, 2015] and a few other GCMs [Held and Zhao, 2008; Becker and Stevens, 2014; Shi and Bretherton, 2014; Reed *et al.*, 2015] also occurs in this GCM. Consistently with other studies, self-aggregation exhibits a dependence on surface temperature [e.g., Khairoutdinov and Emanuel, 2010; Wing and Emanuel, 2014], and the mechanisms primarily responsible for its initiation depend on the range of SST considered [e.g., Wing and Cronin, 2015]. The role of cloud radiative effects and WISHE in the initiation of self-aggregation has been pointed out in most studies. However, the temperature dependence, as well as the physical mechanisms which dominate the triggering of self-aggregation at a given SST, sometimes differ significantly from one model to the next. For instance, in contrast to Wing and Emanuel [2014], we find no evidence in our model of a critical role played by the absorption of SW radiation by water vapor in the triggering of self-aggregation. In contrast with several CRM studies [Bretherton *et al.*, 2005; Muller and Held, 2012; Muller and Bony, 2015], the shallow circulation that develops between dry and moist areas does not contribute to self-aggregation in our model by transporting MSE up-gradient (Figure 7). Instead, self-aggregation relates to the strengthening and expansion of the radiatively driven cold pools that progressively isolate the deep convection and force it to occur in increasingly narrow areas. Finally, in contrast to other studies [Muller and Held, 2012; Wing and Emanuel, 2014; Wing and Cronin, 2015], high-cloud radiative effects are also necessary for the triggering of self-aggregation at all SSTs.

These differences can arise from different factors. Some processes present in CRMs may not be represented by GCMs (e.g., the impact of the mesoscale organization of shallow convection on surface winds, and therefore the role of WISHE in subsidence areas). The representation of low-level clouds and of their radiative effects can also play an important role: the sensitivity of the low-cloud fraction to surface temperature (i.e.,

the strength of the low-cloud feedback) is known to be vastly different across models [Bony and Dufresne, 2005; Sherwood et al., 2014], and therefore the role that low-cloud radiative effects play in the triggering of self-aggregation at any given SST can also differ across models.

In this context, observational investigations of the interplay between low clouds, cold pools, surface fluxes and shallow circulations in the lower troposphere, its dependence on SST, and the role that it may play in the organization of deep convection, would be highly welcome. Is there evidence for the formation of “radiatively driven” cold pools in the dry areas of the tropics? Is the organization of shallow convection such as studied with Large-Eddy Simulation models [Seifert and Heus, 2013] sufficient to produce cold pools in non-convective regions of the tropics and influence the remote organization of deep convection? Can the sensitivity of low-level clouds to surface temperature, which is found to play such a critical role in the temperature dependence of self-aggregation in this model, be constrained by observations? Some of these questions might be answered by extending to the trade wind regions of the tropics studies such as the one carried out over the Indian Ocean by Feng et al. [2015], and by developing observing networks such as the one discussed by Stevens et al. [2015].

In the meantime, the evidence for the presence of a self-aggregation behavior in a large range of numerical models makes us wonder what role this phenomenon may play in climate. How much does it affect the large-scale circulation of the atmosphere in realistic model configurations? What role does it play in the ability of the model to predict Madden-Julian Oscillations, or in Climate Sensitivity? GCMs constitute convenient tools to address these questions, and the present model will be used to carry out some of these investigations.

Acknowledgments

We thank Caroline Muller, Allison Wing, Bjorn Stevens, Jean-Yves Grandpeix, and Catherine Rio for many useful discussions during the development of this work as well as two anonymous reviewers for their insightful comments. We acknowledge the Institut du développement et des ressources en informatique scientifique (IDRIS) for computational resources and support from UPMC (Université Pierre et Marie Curie), CNRS (the French National Center for Scientific Research), and the Labex L-IPSL.

References

- Arnold, N. P., and D. A. Randall (2015), Global-scale convective aggregation: Implications for the MJO, *J. Adv. Model. Earth Syst.*, in press.
- Becker, T., and B. Stevens (2014), Climate and climate sensitivity to changing CO₂ on an idealized land planet, *J. Adv. Model. Earth Syst.*, 6, 1205–1223, doi:10.1002/2014MS000369.
- Bony, S., and J.-L. Dufresne (2005), Marine boundary layer clouds at the heart of tropical cloud feedback uncertainties in climate models, *Geophys. Res. Lett.*, 32, L20806, doi:10.1029/2005GL023851.
- Bony, S., and K. A. Emanuel (2001), A parameterization of the cloudiness associated with cumulus convection; Evaluation using TOGA COARE data, *J. Atmos. Sci.*, 58(21), 3158–3183, doi:10.1175/1520-0469(2001)058<3158:APOTCA>2.0.CO;2.
- Bony, S., et al. (2015), Clouds, circulation and climate sensitivity, *Nat. Geosci.*, 8(4), 261–268, doi:10.1038/ngeo2398.
- Bretherton, C. S., P. N. Blossey, and M. Khairoutdinov (2005), An energy-balance analysis of deep convective self-aggregation above uniform SST, *J. Atmos. Sci.*, 62(12), 4273–4292, doi:10.1175/JAS3614.1.
- Brient, F., and S. Bony (2012), Interpretation of the positive low-cloud feedback predicted by a climate model under global warming, *Clim. Dyn.*, 40(9–10), 2415–2431, doi:10.1007/s00382-011-1279-7.
- Bryan, G. D., Ahijevych, C. Davis, S. Trier, and M. Weisman (2005), Observations of cold pool properties in mesoscale convective systems during BAMEX, paper presented at 32nd Conference on Radar Meteorology/11th Conference on Mesoscale Processes, Am. Meteorol. Soc., Albuquerque, N. M.
- Deardorff, J. W. (1972), Theoretical expression for the countergradient vertical heat flux, *J. Geophys. Res.*, 77(30), 5900–5904, doi:10.1029/JC077i030p05900.
- Dufresne, J.-L., et al. (2013), Climate change projections using the IPSL-CM5 Earth System Model: From CMIP3 to CMIP5, *Clim. Dyn.*, 40(9–10), 2123–2165, doi:10.1007/s00382-012-1636-1.
- Emanuel, K., A. A. Wing, and E. M. Vincent (2014), Radiative-convective instability, *J. Adv. Model. Earth Syst.*, 6, 75–90, doi:10.1002/2013MS000270.
- Emanuel, K. A. (1987), An air-sea interaction model of intraseasonal oscillations in the tropics, *J. Atmos. Sci.*, 44(16), 2324–2340.
- Emanuel, K. A. (1993), A cumulus representation based on the episodic mixing model: The importance of mixing and microphysics in predicting humidity, in *The Representation of Cumulus Convection in Numerical Models*, Meteorol. Monogr., edited by K. A. Emanuel and D. J. Raymond, 24(46), pp. 185–192, Am. Meteorol. Soc.
- Feng, Z., S. Hagos, A. K. Rowe, C. D. Burleyson, M. N. Martini, and S. P. de Szoeke (2015), Mechanisms of convective cloud organization by cold pools over tropical warm ocean during the AMIE/DYNAMO field campaign, *J. Adv. Model. Earth Syst.*, 7, 357–381, doi:10.1002/2014MS000384.
- Fermepin, S., and S. Bony (2014), Influence of low-cloud radiative effects on tropical circulation and precipitation, *J. Adv. Model. Earth Syst.*, 6, 513–526, doi:10.1002/2013MS000288.
- Grandpeix, J.-Y., and J.-P. Lafore (2009), A density current parameterization coupled with Emanuel's convection scheme. Part I: The models, *J. Atmos. Sci.*, 67(4), 881–897, doi:10.1175/2009JAS3044.1.
- Held, I. M., and M. Zhao (2008), Horizontally homogeneous rotating radiative convective equilibria at GCM resolution, *J. Atmos. Sci.*, 65(6), 2003–2013, doi:10.1175/2007JAS2604.1.
- Held, I. M., R. S. Hemler, and V. Ramaswamy (1993), Radiative-convective equilibrium with explicit two-dimensional moist convection, *J. Atmos. Sci.*, 50(23), 3909–3927, doi:10.1175/1520-0469(1993)050<3909:RCEWET>2.0.CO;2.
- Held, I. M., M. Zhao, and B. Wyman (2007), dynamic radiative convective equilibria using GCM column physics, *J. Atmos. Sci.*, 64(1), 228–238, doi:10.1175/JAS3825.11.
- Hourdin, F., et al. (2006), The LMDZ4 general circulation model: Climate performance and sensitivity to parametrized physics with emphasis on tropical convection, *Clim. Dyn.*, 27(7–8), 787–813, doi:10.1007/s00382-006-0158-0.

- Hourdin, F., et al. (2012), Impact of the LMDZ atmospheric grid configuration on the climate and sensitivity of the IPSL-CM5a coupled model, *Clim. Dyn.*, *40*(9-10), 2167–2192, doi:10.1007/s00382-012-1411-3.
- Houze, R. A. (2004), Mesoscale convective systems, *Rev. Geophys.*, *42*, RG4003, doi:10.1029/2004RG000150.
- Jeevanjee, N., and D. M. Romps (2013), Convective self-aggregation, cold pools, and domain size, *Geophys. Res. Lett.*, *40*, 994–998, doi:10.1002/grl.50204.
- Khairoutdinov, M., and K. Emanuel (2010), Aggregation of convection and the regulation of tropical climate, paper presented at 29th Conference on Hurricanes and Tropical Meteorology, Am. Meteorol. Soc., Tucson, Ariz.
- Khairoutdinov, M., and K. Emanuel (2012), The effects of aggregated convection in cloud-resolved radiative-convective equilibrium, paper presented at 30th Conference on Hurricanes and Tropical Meteorology, Am. Meteorol. Soc., Ponte Vedra Beach, Fla.
- Khairoutdinov, M., and K. Emanuel (2013), Rotating radiative-convective equilibrium simulated by a cloud-resolving model, *J. Adv. Model. Earth Syst.*, *5*, 816–825, doi:10.1002/2013MS000253.
- Lafore, J.-P., and M. W. Moncrieff (1989), A numerical investigation of the organization and interaction of the convective and stratiform regions of tropical squall lines, *J. Atmos. Sci.*, *46*(4), 521–544, doi:10.1175/1520-0469(1989)046<0521:ANIOTO>2.0.CO;2.
- Lott, F. (1999), Alleviation of stationary biases in a GCM through a mountain drag parameterization scheme and a simple representation of mountain lift forces, *Mon. Weather Rev.*, *127*(5), 788–801, doi:10.1175/1520-0493(1999)127<0788:AOSBIA>2.0.CO;2.
- Madden, R. A., and P. R. Julian (1994), Observations of the 4050-day tropical oscillation: a review, *Mon. Weather Rev.*, *122*(5), 814–837, doi:10.1175/1520-0493(1994)122<0814:OOTDIO>2.0.CO;2.
- Mapes, B. E., and R. A. Houze (1993), Cloud clusters and superclusters over the oceanic warm pool, *Mon. Weather Rev.*, *121*(5), 1398–1416, doi:10.1175/1520-0493(1993)121<1398:CCASOT>2.0.CO;2.
- Mauritsen, T., and B. Stevens (2015), Missing iris effect as a possible cause of muted hydrological change and high climate sensitivity in models, *Nat. Geosci.*, *8*, 346–351, doi:10.1038/ngeo2414.
- Morcrette, J.-J. (1991), Radiation and cloud radiative properties in the European Centre for Medium Range Weather Forecasts forecasting system, *J. Geophys. Res.*, *96*(D5), 9121–9132, doi:10.1029/89JD01597.
- Muller, C., and S. Bony (2015), What favors convective aggregation and why?, *Geophys. Res. Lett.*, *42*, 5626–5634, doi:10.1002/2015GL064260.
- Muller, C. J., and I. M. Held (2012), Detailed investigation of the self-aggregation of convection in cloud-resolving simulations, *J. Atmos. Sci.*, *69*(8), 2551–2565, doi:10.1175/JAS-D-11-0257.1.
- Nakazawa, T. (1988), Tropical super clusters within intraseasonal variations over the western Pacific, *J. Meteorol. Soc. Jpn.*, *66*(6), 823–839.
- Neelin, J. D., I. M. Held, and K. H. Cook (1987), Evaporation-wind feedback and low-frequency variability in the tropical atmosphere, *J. Atmos. Sci.*, *44*(16), 2341–2348.
- Nolan, D. S., and E. D. Rappin (2008), Increased sensitivity of tropical cyclogenesis to wind shear in higher SST environments, *Geophys. Res. Lett.*, *35*, L14805, doi:10.1029/2008GL034147.
- Nolan, D. S., E. D. Rappin, and K. A. Emanuel (2007), Tropical cyclogenesis sensitivity to environmental parameters in radiative convective equilibrium, *Q. J. R. Meteorol. Soc.*, *133*(629), 2085–2107, doi:10.1002/qj.170.
- Popke, D., B. Stevens, and A. Voigt (2013), Climate and climate change in a radiative-convective equilibrium version of ECHAM6, *J. Adv. Model. Earth Syst.*, *5*, 1–14, doi:10.1029/2012MS000191.
- Reed, K., B. Medeiros, J. Bacmeister, and P. Lauritzen (2015), Global radiative convective equilibrium in the community atmosphere model, version 5, *J. Atmos. Sci.*, *72*(5), 2183–2197, doi:10.1175/jas-d-14-0268.1.
- Rotunno, R., J. B. Klemp, and M. L. Weisman, (1988), A theory for strong, long-lived squall lines, *J. Atmos. Sci.*, *45*, 463–485, doi:10.1175/1520-0469(1988)045<0463:ATFSL>2.0.CO;2
- Seifert, A., and T. Heus (2013), Large-eddy simulation of organized precipitating trade wind cumulus clouds, *Atmos. Chem. Phys.*, *13*(11), 5631–5645, doi:10.5194/acp-13-5631-2013.
- Sherwood, S. C., S. Bony, and J.-L. Dufresne (2014), Spread in model climate sensitivity traced to atmospheric convective mixing, *Nature*, *505*(7481), 37–42, doi:10.1038/nature12829.
- Shi, X., and C. S. Bretherton (2014), Large-scale character of an atmosphere in rotating radiative-convective equilibrium, *J. Adv. Model. Earth Syst.*, *6*, 616–629, doi:10.1002/2014MS000342.
- Stevens, B., et al. (2015), The Barbados Cloud Observatory anchoring investigations of clouds and circulation on the edge of the ITCZ, *Bull. Am. Meteorol. Soc.*, doi:10.1175/BAMS-D-14-00247.1.
- Tobin, I., S. Bony, and R. Roca (2012), Observational evidence for relationships between the degree of aggregation of deep convection, water vapor, surface fluxes, and radiation, *J. Clim.*, *25*(20), 6885–6904, doi:10.1175/JCLI-D-11-00258.1.
- Tobin, I., S. Bony, C. E. Holloway, J.-Y. Grandpeix, G. Sze, D. Coppin, S. J. Woolnough, and R. Roca (2013), Does convective aggregation need to be represented in cumulus parameterizations?, *J. Adv. Model. Earth Syst.*, *5*(4), 692–703, doi:10.1002/jame.20047.
- Tompkins, A. M. (2001), Organization of tropical convection in low vertical wind shears: The role of water vapor, *J. Atmos. Sci.*, *58*(6), 529–545, doi:10.1175/1520-0469(2001)058<0529:OOTCIL>2.0.CO;2.
- Tompkins, A. M., and G. C. Craig (1998), Radiative convective equilibrium in a three-dimensional cloud-ensemble model, *Q. J. R. Meteorol. Soc.*, *124*(550), 2073–2097, doi:10.1002/qj.49712455013.
- Vial, J., J.-L. Dufresne, and S. Bony (2013), On the interpretation of inter-model spread in CMIP5 climate sensitivity estimates, *Clim. Dyn.*, *41*(11-12), 3339–3362, doi:10.1007/s00382-013-1725-9.
- Vial, J., et al. (2015), Coupling between lower-tropospheric convective mixing and low-level clouds: physical mechanisms and dependence on convection scheme, *J. Adv. Model. Earth Syst.*, submitted.
- Wing, A. A., and T. W. Cronin (2015), Self-aggregation of convection in long channel geometry, *Q. J. R. Meteorol. Soc.*, doi:10.1002/qj.2628.
- Wing, A. A., and K. Emanuel (2012), Organization of tropical convection: Dependence of self-aggregation on sst in an idealized modeling study, paper presented at 30th Conference on Hurricanes and Tropical Meteorology, Am. Meteorol. Soc., Ponte Vedra Beach, Fla.
- Wing, A. A., and K. A. Emanuel (2014), Physical mechanisms controlling self-aggregation of convection in idealized numerical modeling simulations, *J. Adv. Model. Earth Syst.*, *6*, 59–74, doi:10.1002/2013MS000269.
- Zhang, M., et al. (2013), CGILS: Results from the first phase of an international project to understand the physical mechanisms of low cloud feedbacks in single column models, *J. Adv. Model. Earth Syst.*, *5*, 826–842, doi:10.1002/2013MS000246.